Rb and Cs broadening of the Na resonance lines

B. Kamke,* W. Kamke,* K. Niemax,† and A. Gallagher‡
Joint Institute for Laboratory Astrophysics, National Bureau of Standards and University of Colorado, Boulder, Colorado 80309
(Received 11 February 1983)

The broadening of the Na resonance lines, due to collisions with Rb and with Cs, has been measured with the use of the normalized fluorescence-intensity method of Chatham, Lewis, and Gallagher. Several Na resonance-radiation diffusion and absorption corrections were necessary in the Rb case, due to an unavoidable excess of Na density in the Rb vapor. The line-broadening rate coefficients k_1 and k_2 for the D_1 and D_2 resonance lines are $k_1(\mathrm{Rb})=(6.2\pm0.4)\times10^{-9}$ cm^{3}s^{-1}, $k_2(\mathrm{Rb})=(5.5\pm0.6)\times10^{-9}$ cm^{3}s^{-1}, $k_1(\mathrm{Cs})=(6.9\pm1.0)\times10^{-9}$ cm^{3}s^{-1}, and $k_2(\mathrm{Cs})=(5.5\pm0.9)\times10^{-9}$ cm^{3}s^{-1} at $T\simeq300$ °C. The leading (C_6R^{-6}) dipole-dipole long-range dispersion forces for the Na-Rb and Na-Cs interactions are calculated, and are used in the impact-theory formula to obtain theoretical line-broadening rate coefficients. These are in poor agreement with the measurements, indicating that as suggested by Vadla, the higher-order (C_8R^{-8}) dispersion terms are also important at the very long range responsible for this line broadening.

I. INTRODUCTION

Collisional interactions between the lower-energy states of alkali-metal atoms are exceptionally strong, long-range forces. The dipole-dipole interaction between an alkali-metal atom in the first excited (nP) state and an identical atom in the ground (nS) state varies as R^{-3} and typically equals kT at $R\cong15$ Å. This resonance-line interaction, which is responsible for resonance broadening and $n^2P_{1/2}\leftrightarrow n^2P_{3/2}$ excitation transfer, is so large that these processes occur at 20–30 Å, where charge overlap and higher-order correlation forces are quite negligible. Thus resonance-broadened line shapes are one of the best-characterized theoretical problems in collisional line shapes,[1–3] as is the fine-structure transition in excitation transfer,[4] although agreement between experiments and calculations is not always satisfactory.[5]

The interaction between an alkali-metal (1) in the first excited (n_1P) state and a different alkali-metal (2) in the ground (n_2S) state is also very strong at long range due to the same resonance-line dipole-dipole forces, but as the excitation energies are no longer identical on the two atoms this interaction occurs as a second-order perturbation, proportional to R^{-6} at long range. In many cases this is still a strong enough interaction to also yield large perturbations before charge overlap occurs, so that this could also be an unusually well-characterized interaction. As the key to analyzing collisional line shape and excitation transfer problems is knowledge of the atomic interactions, these mixed alkali-metal collisions thus offer an intriguing testing ground for line-shape and energy-transfer theories. Furthermore, in this dissimilar alkali-metal case, the resonance-line dipole-dipole interaction leads to monotonically increasing (or decreasing) adiabatic energy differences for all radiating levels associated with each atom, in contrast to the resonance interaction between identical atoms that yield different signs for different Zeeman sublevels. Thus different aspects of line-shape theory, particularly the "antistatic" wing shape, may be investigated in the dissimilar alkali-metal case.

The interaction of the first excited states of dissimilar alkali-metals can be thought of as a repulsion between the two molecular states that separate to $|A\rangle=|(n_1P)(n_2S)\rangle$ and to $|B\rangle=|(n_1S)(n_2P)\rangle$ and are coupled by the dipole-dipole interaction C_3/R^3. When one diagonalizes the resulting interaction matrix:

$$\begin{bmatrix} E_A & C_3R^{-3} \\ C_3R^{-3} & E_B \end{bmatrix}, \tag{1}$$

the energy eigenvalues $E_\pm$ separate as C_6R^{-6} at large R, where $|E_A-E_B|\gg C_3R^{-3}$, and as C_3R^{-3} at small R, where $C_3R^{-3}\gg|E_A-E_B|$. [Here $C_6=C_3^2/(E_A-E_B)$.] The unusually large size of this van der Waals interaction can be seen from this expression for C_6, in which

$$C_3=K(f_A/\Delta E_A)^{1/2}(f_B/\Delta E_B)^{1/2},$$

with f the resonance-line oscillator strength and ΔE its transition energy, K is a constant of unity order of magnitude, and E_A-E_B is the difference in these transition energies. Typically, $f_A\cong f_B\cong1$, $\Delta E_A\cong\Delta E_B\cong$ eV, E_A-E_B varies from 0.7 to 0.05 eV for the various alkali-metal combinations, so that $C_3\cong10$ and $C_6=10^4$–10^5 a.u. results. In comparison, for a typical alkali-metal–inert-gas interaction $\Delta E_B\cong E_B-E_A\cong10$ eV and $f_B\sim0.3$, so that $C_6\sim100$ a.u.

When M_L and M_S levels on both atoms and the fine-structure perturbation are included in the theory, (1) becomes a 24×24 matrix with 16 different eigenvalues as described in Refs. 3 and 4. At small R, these adiabatic states approximately diagonalize into singlet and triplet Π and Σ states, while as $R\to\infty$ they diagonalize into the four fine-structure states with C_6R^{-6} perturbation energies. Thus the adiabatic states and their energies have somewhat complicated behavior, but when E_A-E_B greatly exceeds the fine-structure splitting, as generally occurs (K-Rb is an exception), these group into states of three different energies separating to the fine-structure levels of each atom. Thus, if this resonance-line dipole-dipole interaction were the only strong, long-range interaction, this

would still be a relatively simple, well-understood interaction. However, the higher-state mixings responsible for the normal van der Waals energies of the first excited states must also be considered, as is done in Appendix A. Furthermore, as shown in Ref. 6, the C_8R^{-8} interactions are also very large and important for these mixed alkali metals. Thus the potentials are rather complicated, but their redeeming value is that most of the terms that enter these interactions involve only alkali-metal-atom dipole oscillator strengths that are accurately known. (Some of the C_8 terms may be uncertain.[6]) In addition, the molecular energy terms that are important at closer range are becoming available from calculations.[7,8] Thus these mixed-alkali-metal resonance-line interactions are somewhat complicated, but amenable to calculation.

The energy splitting $E_A - E_B$ is smallest and C_6 largest for the K-Rb interaction, but for experimental reasons we have chosen here to study the Na-Rb and Na-Cs cases. Foremost of these reasons is the difficulty of obtaining sufficiently pure alkali metals to yield, predominantly, perturbations by the dissimilar alkali metals, i.e., strong as the K-Rb interaction is, that for K-K is much stronger and a few percent of K in the Rb can obscure the spectrum of K-Rb by that of K-K. To minimize the self-broadening, the present experiments were carried out by distilling high-purity Rb or Cs into a cell and scattering laser light from the inevitable Na impurities. (Beuc, Movre, and Vadla[6] have recently succeeded in measuring the Cs broadening of K with a similar approach.) At the typical Rb operating density of $\sim 10^{16}$ cm^{-3}, the Na density was typically $\sim 10^{12}$ cm^{-3}. This was much more Na than desired, but not so much that the Na-Na absorption obscured the Na-Rb absorption being measured. A considerably lower Na density was achieved in Cs of $\sim 10^{16}$ cm^{-3} density, so that the Cs-broadening experiment was relatively straightforward. The secondary, well-known reason for choosing Na-Rb and Na-Cs is, of course, the match of the Na resonance lines with a Rhodamine-6G dye laser.

II. EXPERIMENT AND MEASUREMENTS

These measurements of line broadening in the Lorentzian line-core region were based on the method of Chatham *et al.*,[9] in which the fluorescence intensity is measured while tuning a laser across the line core. Reiterating briefly, the fluorescent intensity $I(\nu)$ is proportional to the absorption coefficient $k(\nu)$, so that

$$I(\nu)\Big/\int I(\nu')d\nu' = k(\nu)\Big/\int k(\nu')d\nu' .$$

Furthermore,[9] $k(\nu)$ for a frequency ν in the line wing equals $\Gamma_{\rm tot}(2\pi\Delta\nu)^{-2}\int k(\nu')d\nu'$, where $\Delta\nu = \nu - \nu_{\rm atomic}$. Thus

$$\Gamma_{\rm tot} = \Gamma_N + \Gamma_{\rm Br} = (2\pi\Delta\nu)^2 I(\nu)\Big/\int I(\nu')d\nu' . \quad (2)$$

Here $\Gamma_{\rm Br} = k_{\rm Br}n$, where n is the perturber density and $k_{\rm Br}$ the desired broadening rate coefficient. One measures $I(\nu)$ for a range of ν outside the Doppler region, but within the region of validity of the impact approximation, generally 5—15 GHz from the line center. A small asymmetry term as well as a shift of the line center of $k(\nu)$ also occurs,[10,11] but these have a negligible effect on the linewidth (less than 1% for 5—15 GHz detuning) and can be ignored in broadening measurements. Thus a plot of $(2\pi\Delta\nu)^2 I(\nu)/\int I(\nu')d\nu'$ vs n has a slope $k_{\rm Br}$.

These expressions apply to optically thin vapor in which the laser beam and fluorescence are not attenuated or diffused. In the Na-Cs experiment the Na resonance lines were nearly optically thin and only minor corrections for laser attenuation were necessary. This experiment will be described in Sec. II A. The Na density was much higher in the Rb experiment, so that major optical depth corrections were necessary even with a very narrow cell. This experiment is described in Sec. II B. In both experiments we measured the perturber (Rb or Cs) density by the equivalent-width method.[12]

A. Na-Cs measurements

For the experiment Cs was distilled into a 5-cm diameter, 5-cm wide cylindrical Pyrex cell, which was then sealed off with a $\sim$1-cm diameter, $\sim$10-cm long sidearm. This cell was operated in an area with a slightly lower sidearm temperature and the Cs density, n, was measured at each temperature by the equivalent-width method,[12] i.e., as indicated in Fig. 1, we measured the transmitted spectrum for wavelength around the Cs D_2 resonance line to obtain the absorption equivalent width $W = \int_0^\infty d\lambda[1 - T(\lambda)]$, where $T(\lambda)$ is the cell transmission.

If, as in the present case, $T(\lambda) \cong 1$ in the Lorentzian line wing of the Voigt profile, W is essentially identical to that of a pure Lorentzian line, since $1 - T(\lambda) \cong 0$ in the line core where the hfs and Doppler broadening influence the line shape. (This approximation is calculated to be accurate to better than 1% in the present case.)

For the Lorentzian line-wing absorption coefficient of

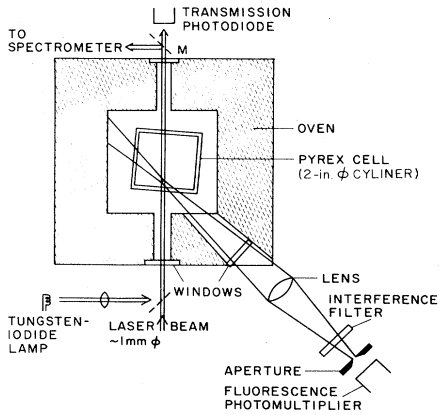

FIG. 1. Cross section of the cell and optics used in the Cs broadening experiment. The cell cylinder axis is slightly away from parallel to the laser beam, to separate reflections, and fluorescence from $\sim$3 mm into the cell was detected to avoid scattered light at the window. A pair of removable mirrors (dashed-lines, M) indicate the alternate measurement of Cs absorption equivalent width. The interference filter passed $\sim$100 Å centered on the Na D lines.

$$k(\nu-\nu_0)=\frac{\lambda^2}{8\pi}\frac{g_2}{g_1}\frac{\Gamma_N\Gamma_T n}{4\pi^2(\nu-\nu_0)^2}\ , \tag{3a}$$

one obtains

$$W=\int d\lambda(1-e^{-k(\lambda)L})=\frac{\lambda^3}{c}\left[\frac{\Gamma_n\Gamma_T L n g_2}{8\pi^2 g_1}\right]^{1/2}\ . \tag{3b}$$

Taking $\Gamma_T=k_{\mathrm{Br}}n$, with $k_{\mathrm{Br}}=\lambda^3 g_2\Gamma_N k_s/8\pi^2 g_1$ as in Ref. 2, Eq. (3b) becomes

$$W=\left[\frac{\lambda^{4.5}\Gamma_N g_2\sqrt{k_s L}}{2.37\times10^4 g_1}\right]n\ , \tag{4}$$

where λ and the cell thickness L are given in centimeters, n in inverse cubic centimeters, and W in angstroms. For the present case of Cs D_2-line self-broadening, we use $k_s=1.47$ from Table I of Ref. 2 to obtain

$$W=2.06\times10^{-15}L^{1/2}(n_{\mathrm{Cs}})\ , \tag{5}$$

where L is given in centimeters, n in inverse cubic centimeters, and W in angstroms. This calculation[2] of k_s has been verified to $\pm15\%$ by Huennekens and Gallagher,[13] but it is expected to be considerably more accurate than that. The value of Γ_N for the Cs resonance line is uncertain to $\sim3\%$. The Cs density measured by this method is accurate to $\sim7\%$, with the uncertainty due primarily to baseline uncertainty in measuring W for these very-broad lines. The resulting Cs density (at 10^{16} cm^{-3}) was a factor of 2 below the value suggested by Nesmeyanov,[14] who compromised between several measurements, but within 5% of the value measured by Taylor and Langmuir (reported in Ref. 14). However, as noted in Ref. 12, it is important to have a well-saturated cell to obtain equilibrated vapor pressures.

In order to minimize radiation trapping effects, fluorescence was detected from a region just inside the cell window as shown in the cross section in Fig. 1. Fluorescence from both D lines was detected in this experiment, while the laser was tuned across each D line separately. Here the length of the cell traversed by the laser beam was ~50 mm, while that to the detected volume was ~3 mm. Thus the transmission $T(\nu)$ of the laser beam to the scattering volume is given by $[T_c(\nu)]^{\epsilon}$, where $T_c(\nu)$ is the measured transmission through the cell and $\epsilon=\frac{3}{50}$. The measured fluorescent intensity I in the line core is proportional to $k(\nu)T(\nu)$, so we correct Eq. (2) for this minor attenuation using

$$\Gamma_{\mathrm{tot}}=\frac{(2\pi\Delta\nu)^2k(\nu)}{\int k(\nu')d\nu'}=\frac{(2\pi\Delta\nu)^2I(\nu)}{\int I(\nu')[T_c(\nu)]^{-\epsilon}d\nu'}\ . \tag{6}$$

In this procedure we have assumed that the transmission of the fluorescence, through ~3 mm of vapor to the detector is independent of the laser wavelength, which is only valid when $\Gamma_{\mathrm{Br}}\gg\Gamma_N$, and there is complete redistribution. In the experiment the Na optical depth was only significant at the higher temperatures where Γ_{Br} due to Cs collisions did exceed Γ_N, and most of the fluorescence was redistributed. Furthermore, even at these highest temperatures the optical depth correction in Eq. (2) was less than a 10% total correction, so further corrections due to lack of complete redistribution were deemed $<2\%$. Since both D lines were detected, $3P_{1/2}\leftrightarrow3P_{3/2}$ excitation transfer has no effect on the results.

Several 30 GHz scans across each Na resonance line were used to obtain the ratio of I at 5–20 GHz in the Lorentzian wing to $\int I(\nu')d\nu'$ across the line core. Baseline corrections, due to scattered light, were relatively minor and determined by tuning the laser far from the resonance lines. Minor laser-intensity variations were corrected by a voltage divider. From 5–10 GHz detuning $k(\nu)$ exceeds the purely Lorentzian value due to hfs and Doppler broadening for the Na resonance lines (e.g., see Ref. 9, Fig. 1). This is a fractional correction of 1–10% that has been calculated and applied to the measured I in the 5–10 GHz region, resulting in nearly a constant value for $(\Delta\nu)^2I(\nu)$ for the studied detunings of 5–15 GHz.

The reduced data for Γ_T vs Cs density is given in Fig. 2. Fitting this data to $\Gamma_T=\Gamma_N+k_{\mathrm{Br}}n_{\mathrm{Cs}}$, we obtain $k_{\mathrm{Br}}=6.9\times10^{-9}$ cm^{3}s^{-1} for the Na D_1 line, broadening rate coefficient, and $k_{\mathrm{Br}}=5.5\times10^{-9}$cm^{3}s^{-1} for the D_2 line. The uncertainty in the data of Fig. 2 is estimated at $\sim7\%$. The rate coefficients are also uncertain by $\sim7\%$ due to the Cs density scale. An additional significant source of uncertainty in this Cs-broadening experiment is a laser scanning nonlinearity that was not systematically corrected for, as it was in the following Rb-broadening experiment. This scanning nonlinearity introduces $\sim10\%$ uncertainty into the measured Γ_T values. A minor asymmetry in the line shape does not introduce uncertainty in the width as its effect is second order in the magnitude of the asymmetry parameter. Thus, yielding these sources of uncertainty in quadrature, we obtain the $\sim15\%$ total uncertainties in Table I.

B. Na-Rb measurements

Owing to the large Na impurity fraction in our Rb and the resultant high Na resonance-line optical depths, these measurements were done with a Pyrex cell with reentrant windows to obtain a narrow (1.45 mm) gap between the windows. A schematic diagram of the cell and apparatus is given in Fig. 3. "Pure" Rb was distilled into the cell and sidearm, which was then sealed under vacuum. In this experiment we measured and corrected for the laser scanning nonlinearity, using signals from a 750 MHz

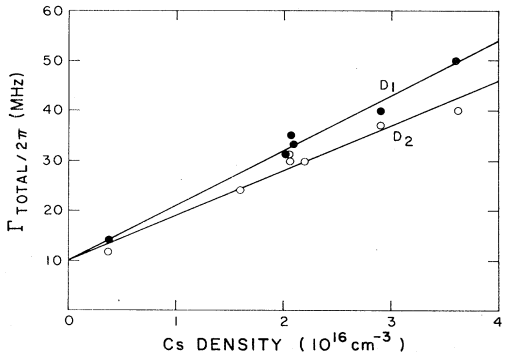

FIG. 2. Measured Na D_1-line (●) and D_2-line (○) total Lorentzian widths, in frequency units, vs Cs density. The fitted lines correspond to the reported broadening rate coefficients, and $\Gamma_N/2\pi=10$ MHz without collisional broadening.

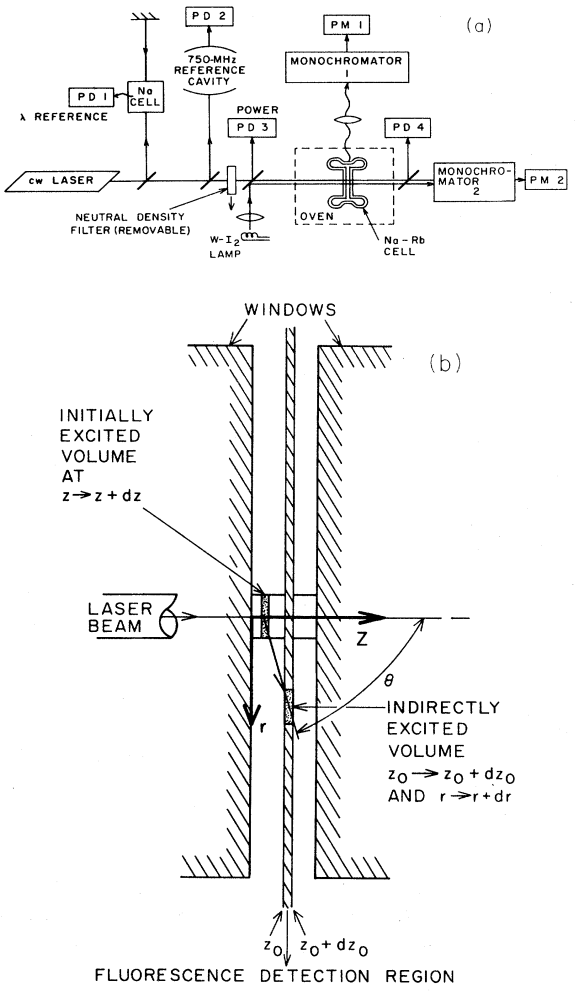

FIG. 3. (a) Schematic diagram of the apparatus for the Na-Rb experiment. The Na cell fluorescence detected by photodiode 1 obtained ν_0 of the D lines from the saturated absorption signals. Nonlinearities in the laser wavelength scan were measured and corrected using the 750 MHz reference cavity and photodiode 2. The D_1- or D_2-line fluorescence from the Pyrex cell was detected with monochromator 1 and photomultiplier 1, and normalized to the incident laser power (photodiode 3). The transmitted laser light was detected by photodiode 4, and the transmitted continuum from the tungsten iodide lamp was scanned by monochromator 2. The laser beam followed the axis of the cylindrically symmetric Pyrex Na-Rb cell. (b) A cross section of the cell interior. The windows of this cell were approximately 12.5 mm diameter with 1.45 mm spacing. A 6-mm diameter, 15-cm long cell sidearm projected (out of the page) from the oven, of temperature T_1, to a second oven, of temperature T_R; typically $T_1 \cong T_R + 20$ K. Fluorescence propagating out the side of the cell (bottom of the figure) from the cross-hatched region z_0 to $z_0 + dz_0$ was measured.

reference cavity (Fig. 3).

In order to minimize scattered light and some complications to the radiation diffusion corrections for this experiment, we detected fluorescence from the D_2 line when scanning the D_1 line, and vice versa. This fluorescence results from fine-structure changing collisions with the Rb. As this collisional rate is independent of the laser frequency, in the absence of radiation trapping the resulting signal is proportional to $k(\nu)$. Corrections are made for a small sloping background signal due to spectrometer leakage of laser scattering plus photomultiplier dark current. This background signal, obtained by tuning the laser off-resonance, is shown in Fig. 4 as line B.

Typically, the fluorescence signal $I(\nu)$ from the center of the cell [z_0 halfway between the windows in Fig. 3(b)] was measured simultaneously with the cell transmission $T_c(\nu)$. Since the laser intensity at the center of the cell is proportional to $T_c^{1/2}$, we then used $\epsilon = \frac{1}{2}$ in the integral of Eq. (6) for this experiment. This procedure is demonstrated in Fig. 4 for a case with $\epsilon = 0.6$.

The measured values of Γ_T must also be corrected for the effect of radiation trapping and diffusion. This correction, which ranges from 3—25%, is calculated in Appendix A. It results from the fact that we detect light from the central region between the windows, and this arises from excitation of atoms in this region by radiation diffusion from other regions, as well as from the direct excitation by the laser radiation [see Fig. 3(b)] [Eq. (2) assume only the direct excitation]. The reason this causes a correction to Γ_T is that the relative contribution of the radiation diffusion part of $I(\nu)$ depends on the laser frequency, so that it adds a different correction in the line core than in the line wing. This in turn results primarily from two factors. (1) When the laser frequency is in the line wing, the Rayleigh scattering at the laser frequency escapes the cell, whereas when it is in the line core it does not. (2) When the laser is severely attenuated the fraction absorbed in the center of the cell relative to the entire cell changes, so that the ratio of radiation diffusion to direct excitation changes as the laser tunes to the line core. These effects are evaluated in Appendix A for our cell geometry and optical depth conditions. The resulting correction factor C is given in Table II.

An additional minor correction, due to reflection of the laser beam from the back windows, is included in the corrections in Appendix A. Since the laser beam is attenuated when tuned on resonance, the intensity of this reflected beam is ν dependent. Allowing for this effect (Appendix A) changes the correction factor C, typically by $\sim 5\%$, to a final factor G. The corrected $\Gamma_T/2\pi$, obtained by multiplying Γ_T from Eq. (2) by this correction factor G, are given in Table II. The resulting corrected $\Gamma_T/2\pi$ are plotted vs n_{Rb} in Figs. 5 and 6. Fitting a straight line to these data yields $\Gamma_T = \Gamma_N + k_{\mathrm{Br}} n_{\mathrm{Rb}}$ with $k_{\mathrm{Br}} = (6.2 \pm 0.4) \times 10^{-9}$ cm^3 s^{-1} for the Na D_1 line and $k_{\mathrm{Br}} = (5.5 \pm 0.6) \times 10^{-9}$ cm^3 s^{-1} for the D_2 line, as reported in Table I. The principal source of these uncertainties is the optical-depth correction. Secondary uncertainties are due to the Rb density determination ($\sim 4\%$), residual scanning nonlinearity problems (1%), baseline and asymmetry correction issues (2%), and statistical noise (1%).

The Rb density used in Figs. 5 and 6 was obtained from the equivalent width of the 7800 Å Rb resonance line absorption, by scanning the cell transmittance of a tungsten-lamp continuum (Figs. 3 and 4). At the $n_{\mathrm{Rb}} \sim 10^{16}$ cm^{-3} region of interest, the Rb self-broadened wings dominate the equivalent width. A calculation including the Rb hfs and isotope shifts confirms that the single Lorentzian-line result [Eq. (4)] is accurate to better

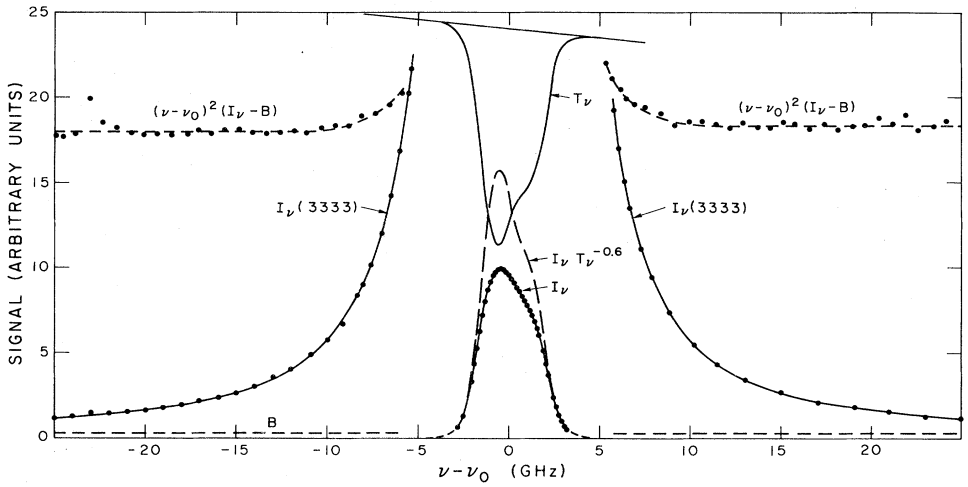

FIG. 4. Example of the data for $n_{Rb}=1.37\times10^{16}$ cm^{-3}, obtained by scanning the D_1 line and detecting D_2 fluorescence from a z_0 position 60% of the distance through the cell ($\epsilon=0.6$). The cell transmission $T_c(\nu)$, labeled T_ν, is used to correct the line-center fluorescence signal $I(\nu')$, labeled I_n, to $I_nT_\nu^{-0.6}$ (dashed line) corresponding to a constant laser intensity at z_0. The quantity $(\nu-\nu_0)^2(I_\nu-B)$, due to the Lorentzian wing of the absorption coefficient, should reach the same constant value on both wings at $|\nu-\nu_0|>10$ GHz if there is no asymmetry to the broadening; the $\sim2\%$ difference is typical and essentially random between data sets. The points near -23 GHz are influenced by Na_2 fluorescence.

than 1% for $n_{Rb}>10^{16}$ cm^{-3}. Equation (4) yields for the Rb D_2 line

$$W=1.24\times10^{-15}L^{1/2}(n_{Rb})\,, \tag{7}$$

where the units of n_{Rb}, L, and W are as in Eq. (5). The n_{Rb} in the cell that we obtain from these measurements are $\sim10\%$ above those calculated from the vapor-pressure relation of Nesmeyanov,[14] when we use the cell sidearm temperature, which was generally ~20 K less than the main cell temperature. Thus, as has been found previously,[15] an evacuated Pyrex cell can yield well-equilibrated Rb vapor pressures. However, for these high Rb density experiments it is important to load a major part of a gram of Rb into the cell, as it is continually being absorbed into the cell walls as they gradually turn brown.

The broadening of the Na resonance lines by Rb was only ~30 MHz at the highest n_{Rb}, so that any line shift is expected to be less than 30 MHz and not very discernible compared to the 3000 MHz Doppler and hyperfine width of the D lines. However, for these relatively slow, long-range collisions considerable asymmetry would arise in the wing-absorption coefficients at the ±25 GHz limits of the line-core scans.[10,11] Nonetheless, we have found very little asymmetry in these wings. If $k(\nu)$ is expressed as

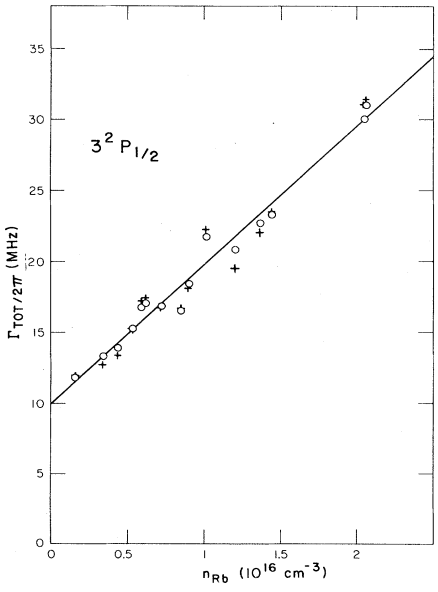

FIG. 5. Measured full Lorentzian linewidth, $\Gamma_{tot}/2\pi$, in frequency units vs Rb density for the Na D_1 line. Points (+) are from data 10—25 GHz on the positive detuning line wing, and (○) from the negative detuning line wing. The straight line is a linear least-squares fit to the data.

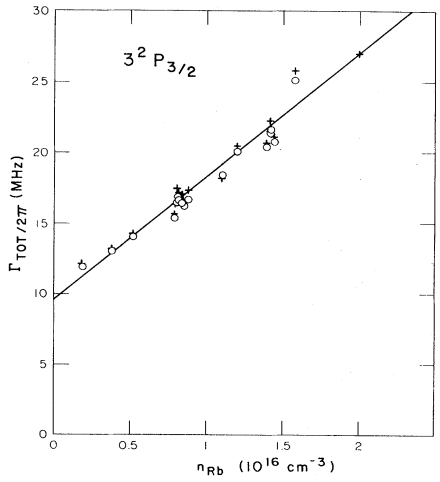

FIG. 6. Same as Fig. 4 for the Na D_2 line.

TABLE I. Na D-line broadening rate coefficients.

D line	Perturber	Measured k (10^{-9} cm^{3}s^{-1})	Calculated k (10^{-9} cm^{3}s^{-1})
D_1	Rb	6.2±0.4	11.3
D_2	Rb	5.5±0.6	11.3
D_1	Cs	6.9±1.0	9.0
D_2	Cs	5.5±0.9	9.0

$K(1+a\,\Delta\nu)/(\Delta\nu)^2$ for $\Delta\nu=10$—100 GHz, then the data plotted in Fig. 4 would be proportional to $(1+a\,\Delta\nu)$. From the data in that figure, and others that are similar, it is apparent that there is less than $\sim 2\%$ asymmetry at $\Delta\nu=\pm 25$ GHz, or that $a<5\times10^{-4}$ GHz^{-1}.

III. DISCUSSION OF RESULTS

The Na*-Rb and Na*-Cs adiabatic potentials given in Appendix B can be used to calculate line-broadening rate coefficients if the nonadiabatic couplings of the J, M_J states are ignored. The Weisskopf radius, where the optical phase shift is unity and most of the impact-broadening occurs, is $\sim 33a_0$. At this distance the excited and ground-state interactions are 0.2 to 1 cm^{-1} and should be fairly well described by van der Waals coefficients in J, M_J representation. Under these circumstances we can use the M_J averaged C_6 coefficients for each $3P_J\rightarrow 3S_{1/2}$ line, which from the bottom line of Table II yields $\Delta C_6=C_6(3P_J)_{\rm av}-C_6(3S_{1/2})=-3560$ a.u. for Na-Rb and -2180 a.u. for Na-Cs. Putting these into the well-known equation for line broadening by a C_6R^{-6} interaction[10],

$$k_{\rm Br}=8.08(\bar{v}_{12})^{3/5}\,|\,\Delta C_6/\hbar\,|^{2/5}$$
$$=1.51\times10^{-10}(T/\mu)^{0.3}\,|\,\Delta C_6\,|^{0.4}\,, \qquad (8)$$

where T is the temperature given in degrees Kelvin and μ is the reduced mass in amu, ΔC_6 is given in atomic units, and $k_{\rm Br}$ is in units of cm^3/s. We calculate the broadening rate coefficients given in column 4 of Table I.

The calculated Cs and Rb broadening rate coefficients are compared to the measured values in Table I, where it is seen that they are $\sim 50\%$ and 100% larger, respectively. This implies that these calculated potentials are not reliable even in the large-R region ($>30a_0$) responsible for the line-core broadening. Furthermore, we do not observe significant asymmetry in the Na-Rb case (we did not investigate this for Na-Cs), whereas major blue asymmetry would be expected for these long-range repulsive interactions. Beuc *et al.*[6] have recently reported measurements of the broadening and line-wing shapes for K-Cs collisions. Their results are consistent with calculated C_6R^{-6} (repulsive) interaction potentials.

Vadla[16] has calculated C_8R^{-8} terms for the Na-Rb and Na-Cs interactions, and he finds these to be comparable to the C_6R^{-6} terms considered here, even at very large R ($\sim 30a_0$). This is partly due to the partial cancellation of the different contributions to C_6R^{-6}, as seen in Table III. These C_8R^{-8} terms are attractive, so that they decrease the magnitude of the Na*-Rb perturbation at large R, and thereby decrease the expected broadening rate coefficient toward the measured values. These interactions are apparently also consistent with the absence of Na*-Rb asymmetry observed here, as they imply a small ΔV at $R>30a_0$, followed by rapid changes in ΔV at smaller R. Of course, when C_8R^{-8} terms exceed C_6R^{-6} terms, it is also necessary to consider still higher-order terms, and it is not clear that this electrostatic expansion is useful at $R<30a_0$. Thus we conclude from these measurements and Vadla's C_8 calculations that this long-range dissimilar—alkali-metals interaction is quite complicated, and not yet understood in spite of its very-long-range character.

ACKNOWLEDGMENTS

Two of the authors (W.K. and K.N.) wish to acknowledge financial support by the Deutsche

TABLE II. Na-Rb linewidth measurements.

$n_{\rm Rb}$ (10^{16} cm^{-3})	D line excited	$\Gamma_{\rm tot}/2\pi$ (MHz) direct scattering +Det	$\Gamma_{\rm tot}/2\pi$ (MHz) direct scattering −Det	Transmission at D-line peak	G	C	Corrected $\Gamma_{\rm tot}/2\pi$ (MHz) +Det	Corrected $\Gamma_{\rm tot}/2\pi$ (MHz) −Det
0.59	D_1	16.5	16.1	0.91	1.04	1.05	17.2	16.7
1.57	D_1	25.6	25.6	0.76	1.04	1.06	26.7	26.7
2.06	D_1	29.1	28.6	0.33	1.05	1.11	30.5	30.1
2.05	D_1	28.6	27.6	0.26	1.06	1.13	30.1	29.2
1.20	D_1	18.0	19.4	0.63	1.08	1.11	19.6	20.9
0.72	D_1	15.6	15.7	0.79	1.07	1.09	16.7	16.9
0.33	D_1	11.9	12.5	0.87	1.07	1.08	12.7	13.3
0.15	D_1	11.5	11.5	0.96	1.03	1.03	11.9	11.9
1.58	D_2	23.8	23.2	0.51	1.08	1.12	25.8	25.1
1.10	D_2	16.0	16.0	0.32	1.16	1.23	18.6	18.6
0.37	D_2	11.9	11.9	0.84	1.10	1.11	13.2	13.1
0.79	D_2	13.3	13.0	0.43	1.19	1.25	15.8	15.5
1.10	D_2	16.0	16.0	0.32	1.16	1.23	18.6	18.6
1.44	D_2	18.5	18.3	0.21	1.16	1.25	21.4	21.2
0.80	D_2	14.0	13.9	0.45	1.16	1.22	16.3	16.2
1.41	D_2	19.0	18.9	0.22	1.10	1.18	20.9	20.8

TABLE III. C_6 terms for the Na $3P$ state.

	Li	K	Rb	Cs
D	2 165	3640	3880	4580
S_1	655	1110	1170	1430
S_0	−7 500	−6055	−6060	−5180
$C_6(3P,M_L=0)$	−11 280	−5890	−5510	−2450
$C_6(3P,M_L=1)$	−1 360	980	1240	2480
$C_6(3^2P_{1/2},M_J=\frac{1}{2})$	−4 680	−1310	−1010	835
$C_6(3^2P_{3/2},M_J=\frac{1}{2})$	−7 971	−3600	−3260	−810
$C_6(3^2S_{1/2},M_J=\frac{1}{2})$	1455	2395	2550	3015
$C_6(3^2P_{1/2})-C_6(3^2S_{1/2})$	−6 135	−3705	−3560	−2180

Forschungsgemeinschaft. This work was supported under National Science Foundation Grant No. PHY-79-04928 through the University of Colorado.

APPENDIX A: RADIATION TRAPPING EFFECTS

Here we evaluate the effect of radiation trapping and diffusion on the ratio of the measured $I(\nu)$ with the laser tuned in the line wing vs $\int I(\nu)d\nu$ integrated across the line core. The relevant cell geometry is shown in Fig. 3(b).

We detect fluorescence plus Rayleigh scattering from excited atoms between z_0 and z_0+dz_0 and $r=0$ to a, with $a=6.2$ mm. These excited atoms result from direct excitation of atoms in the laser beam (direct scattering region in Fig. 3(b), plus fluorescence from atoms at $z_0\rightarrow z_0+dz_0$ and all r excited by radiation diffusion. The line-center optical depths across the narrow-cell direction vary from 0 to ~ 1, so that $<\frac{1}{4}$ of the fluorescence from the initially excited atoms is trapped before escaping the cell and $<\frac{1}{4}$ of the resulting diffused fluorescence is trapped a second time. Thus we limit this calculation to a single diffusion step. We also approximate the transmission of each D-line fluorescence, vs distance l in the cell, by a single effective exponential attenuation coefficient k_i [$I_i(l)=I_i(0)\times\exp(-k_i l)$], which is typically $\sim 70\%$ of the peak absorption k_0 for that line.[17] Consistent with this approximation of a single frequency for each D line, we use the same attenuation coefficient for the laser beam when it is tuned to the line-core region. Furthermore, the atoms excited by this single diffusion step are symmetrically distributed about the cell axis and are still relatively concentrated near this axis. Thus we assume that the average probability that fluorescence from these indirectly excited atoms (in $z_0\rightarrow z_0+z_0$) escape to the detector (without trapping) is the same as for the directly excited atoms.

When the laser frequency ν_L is tuned at or near the D_1 line (frequency ν_1), a fraction $a_{1\rightarrow 2}=(\Gamma_{\rm Br}/\Gamma_I)(R_{12}/R)$ of the reemission occurs at the D_2-line frequency ν_2, where $R=R_{12}+R_{21}+\Gamma_T$, Γ_T, $\Gamma_T=\Gamma_N+\Gamma_{\rm Br}$, and R_{ij} is the excitation transfer rate from level i to j ($1=3^2P_{1/2}$, $2=3^2P_{3/2}$). (In using Γ_N here we have ignored a minor decrease in effective radiative rate, due to trapping.) If $\nu_L=\nu_1$, the remaining fraction of the total absorption, $a_{1\rightarrow 1}=1-(\Gamma_{\rm Br}/\Gamma_T)(R_{12}/R)$ is emitted at ν_1. If the laser is in the optically thin wing of the D_1 line, which we define as ν_3, this remaining fraction is divided between the Rayleigh light at ν_3, with intensity $a_{3\rightarrow 3}=\Gamma_N/\Gamma_T$, and D_1 fluorescence of intensity $a_{3\rightarrow 1}=a_{1\rightarrow 1}-a_{3\rightarrow 3}=(\Gamma_{\rm Br}/\Gamma_T)[(R_{21}+\Gamma_T)/R]$. The fraction of emission on D_2, however, remains unchanged in this case ($a_{3\rightarrow 2}=a_{1\rightarrow 2}$). Similarly, $a_{2\rightarrow 1}=(\Gamma_{\rm Br}/\Gamma_T)(R_{21}/R)$ and $a_{2\rightarrow 2}=1-a_{2\rightarrow 1}$.

Thus, when the laser of intensity I_0 is tuned to ν_i and $I_0k_ie^{-k_iz_0}dz_0$ is absorbed in $z_0\rightarrow z_0+dz_0$, the emission $I^i(z_0)dz_0$ from directly excited atoms is given by

$$I^i(z_0)=I_0k_ie^{-k_iz_0}\sum_{j=1}^{3}a_{i\rightarrow j}\delta(\nu-\nu_j)\equiv\sum_j I_j^i(z_0)\delta(\nu-\nu_j)\ , \tag{A1}$$

where the last step defines $I_j^i(z_0)$, and $a_{1\rightarrow 2}=(\Gamma_{\rm Br}/\Gamma_T)(R_{12}/R)$, $a_{1\rightarrow 1}=1-a_{1\rightarrow 2}$, $a_{1\rightarrow 3}=0$, $a_{3\rightarrow 3}=\Gamma_N/\Gamma_T$, $a_{3\rightarrow 2}=a_{1\rightarrow 2}$, and $a_{3\rightarrow 1}=a_{1\rightarrow 1}-a_{3\rightarrow 3}$.

For ν_L at or near the D_1 line the fluorescence at ν_1 and ν_2 is unpolarized, while for ν_L near ν_2 the D_2 fluorescence is only weakly polarized. For ν_L near the D_2 line the Rayleigh scattering is highly polarized, but as this is not reabsorbed or detected, this is of no consequence in the present calculations. Thus all of the light absorbed at $z\rightarrow z+dz$ is assumed emitted isotropically, so that a fraction $\sin\theta\,d\theta/2$ is emitted into $\theta\rightarrow\theta+d\theta$. The ν_j component is attenuated by $\exp(-k_jl)$ in traversing a length $l=[(z-z_0)^2+r^2]^{1/2}$ of vapor to the volume element at $z_0\rightarrow z_0+dz_0$ and $r\rightarrow r+dr$ [see Fig. 3(b)], and a portion $k_jdz_0/\cos\theta$ is absorbed in this indirectly excited volume. Since the cell radius a is much larger than the radius of the laser beam, it is sufficient here to consider all initially excited atoms to be on axis (at $r=0$).

The total direct fluorescence of frequency ν_j that is reabsorbed into $z_0\rightarrow z_0+dz_0$, which we define as $T_j^i(z_0)dz_0$, is thus

$$T_j^i(z_0)dz_0=\frac{k_jdz_0}{2}\int_0^a dr\int_0^D dz\,I_j^i(z)\exp\{-k_j[(z-z_0)^2+r^2]^{1/2}\}\frac{r}{(z-z_0)^2+r^2}\ , \tag{A2}$$

where D is the cell window spacing [Fig. 3(b)]. Combining (A1) and (A2), we obtain

$$T_j^i(z_0)=I_0k_ia_{i\rightarrow j}T(k_i,k_j,z_0)\ , \tag{A3}$$

where

$$T(k_i,k_j,z_0)=\frac{k_j}{2}\int_0^a dr\int_0^D dx\,\exp\{-k_iz-k_j[(z-z_0)^2+r^2]^{1/2}\}\frac{r}{(z-z_0)^2+r^2}\ , \tag{A4}$$

and for convenience in the following, we define

$$Q(k_i,k_j,z_0)=e^{k_iz_0}T(k_i,k_j,z_0)\ . \tag{A4'}$$

Of this diffused light, each component of frequency ν_j that is reabsorbed into $z_0 \rightarrow z_0 + dz_0$ yields a fraction $a_{j\rightarrow m}$ that is refluoresced at ν_m. Combined with (A3), this indirectly excited fluorescence at ν_m is thus

$$I_m^i(z_0)_{\text{diffusion}} = \sum_j T_j^i(z_0) a_{j\rightarrow m} = I_0 k_i \sum_i a_{i\rightarrow j} T(k_i,k_j,z_0) a_{j\rightarrow m} \ . \quad \text{(A5)}$$

In the experiment we detected fluorescence from the unexcited D line to minimize wall-scattered laser light; thus $m=2$ in the present example of ν_L at or near ν_1. Combining the diffused ν_2 light from Eq. (A5) with that from directly excited atoms, from Eq. (A1), we obtain

$$I_2^i(z_0)_{\text{total}} = I_0 k_i e^{-k_i z_0} \left[a_{i\rightarrow 2} + \sum_j^3 a_{i\rightarrow j} Q(k_i,k_j,z_0) a_{j\rightarrow 2} \right] . \quad \text{(A6)}$$

Thus, using $k_3 z_0 \ll 1$,

$$\frac{I_2^3(z_0)_{\text{total}}}{I_2^1(z_0)_{\text{total}}} = \frac{k_3}{k_1 e^{-k_1 z_0}} C(z_0) \quad \text{(A7)}$$

with

$$C(z_0) = \frac{a_{3\rightarrow 2} + \sum_j a_{3\rightarrow j} Q(k_3,k_j,z_0) a_{j\rightarrow 2}}{a_{1\rightarrow 2} + \sum_j a_{1\rightarrow j} Q(k_1,k_j,z_0) a_{j\rightarrow 2}} \ . \quad \text{(A8)}$$

In this Appendix, we have used k_1 to represent $\int k(\nu')d\nu'$ integrated across the $D1$ line, and k_3 to represent $k(\nu)$ in the line wing. Thus the Eq. (A7) factor k_3/k_1 represents $k(\nu)/\int k(\nu')d\nu'$ due to directly excited atoms, equal to $\Gamma_T/4\pi^2(\nu-\nu_1)^2$. The additional factor of $e^{-k_1 z_0}$ is the laser-absorption correction, represented here by the mean value k_1 of the D_1-line absorption coefficient. This correction is actually evaluated, as given in Eq. (6) and described in the text, by taking $\int I(\nu)[T_c(\nu)]^{-\epsilon} d\nu$, where $T_c(\nu)$ is the cell transmission. The factor $C(z_o)$ in Eq. (A7) is the radiation-diffusion correction to $k(\nu)/\int k(\nu')d\nu'$, for ν in the D_1 line wing. Since $T(k_i,k_j,z_0) \rightarrow 0$ as $n \rightarrow 0$ and $a_{3\rightarrow 2} = a_{1\rightarrow 2}$, this correction factor, given in Eq. (A8), approaches 1 as $n \rightarrow 0$. Furthermore, since $k_3 D \ll 1$, the $j=3$ terms in Eq. (A6) can be dropped and $k_3 \rightarrow 0$ taken to obtain

$$C(z_0) = \frac{1 + Q(0,k_2,z_0) a_{2\rightarrow 2} + Q(0,k_1,z_0) a_{3\rightarrow 1}}{1 + Q(k_1,k_1,z_0) a_{1\rightarrow 1} + Q(k_1,k_2,z_0) a_{2\rightarrow 2}} \ . \quad \text{(A9)}$$

$Q(k_i,k_0,z_0)$ is given in Eq. (A4), but the limit $a \rightarrow \infty$ cannot be taken there without a divergence, because we have used an absorption probability of k_j times the path length dl through the $z_0 \rightarrow z_0 + dz_0$ zone, and this is only true if $k_j dl \ll 1$. Instead, we have made use of the approximation $D^2 \ll a^2$ to obtain a series expansion of the integral in Eq. (A4). The function $Q(k_i,k_j,z_0)$ has been evaluated using

$$Q(k_i,k_j,z) = \frac{e^{k_i z}}{2} \left[\ln\left[\frac{a}{z}\right] + u(k_j a) - u(k_j z) \right] + u((k_j - k_i)z) - e^{-k_i(D-z)} \left[\ln\left[\frac{a}{D-z}\right] + u(k_j a) - u(k_j(D-z)) \right] - u((k_j + k_i)(D-z)) + e^{-k_i z} \ln\left[\frac{z}{D-z}\right] , \quad \text{(A10)}$$

where

$$u(x) = \sum_{n=1}^{\infty} \frac{(-x)^n}{n(n!)} \ .$$

Our experimental conditions are $k_1 = k_2/2$, $z_0/D \cong 0.5$, and $k_2 D \leq 1$.

Of course, this correction factor for D_1-line broadening applies to the D_2 line broadening with the exchange of indices 1 and 2. We note that the functions $Q(0,k_j,z_0)$ and $Q(k_1,k_i,z_0)$ increase monotonically with k_j, but they only differ in that the directly excited atoms were distributed evenly in z in $Q(0,k_j,z_0)$ and with exponential attenuation in $Q(k_1,k_j,z_0)$. Thus these functions are identical at small $k_j D$ and they differ typically by only 25% at the largest densities ($k_2 D \cong 1$) of this experiment. On the other hand, $a_{L\rightarrow 1}/a_{l\rightarrow 1} \ll 1$ at small $k_j D$ and this ratio approaches one at the higher densities where $\Gamma_{\text{Br}} > \Gamma_{\text{nat}}$. Thus the numerator and denominator in (A9) are very similar at all relevant densities.

An additional correction is also necessary for obtaining the final Γ_{tot}. This factor is due to the typically $\sim 12\%$ reflection from the windows on the backside of the cell and oven. Since, at the center of the cell, the direct beam is attenuated by $[T_c(\nu)]^{0.5}$ and the reflection is attenuated by $[T_c(\nu)]^{1.5}$, the measured line core $I(\nu)$ in the numerator of Eq. (2) should be divided by 1.12, and $I(\nu')$ in the denominator should actually be divided by $[T_c(\nu')]^{0.5}[1+0.12T_c(\nu')]$, rather than $[T_c(\nu)]^{0.5}$ as in Eq. (6) and Fig. 3. Furthermore, the radiation diffusion correction (A8) must be applied to this reflected-beam excitation as well. These corrections have been made, and overall cause an additional correction of 0—8 % in Γ_{tot}, in the opposite direction to the correction in (A9). The transmission of the cell walls also decreased gradually during the experiment, due to reaction with Rb, decreasing the effective reflection below 12% and changing this correction. The directly measured values of

$$\Gamma_{\text{tot}}/2\pi = k(\nu) 2\pi (\Delta\nu)^2 \Big/ \int k(\nu')[T_c(\nu')^{-0.5} d\nu' \ ,$$

and the correction factor C, are given in Table II. The overall correction factor, due to radiation diffusion plus the reflectivity effect is labeled G and listed in Table II, and the final, corrected $\Gamma_{\text{tot}}/2\pi$ are given in the last column.

APPENDIX B: VAN DER WAALS ENERGIES OF Na 3P STATE

In the long-range region, where there is negligible charge overlap, singlet and triplet states of the diatomic-alkali-metal molecule have essentially the same energy. Furthermore, when the E_A-E_B greatly exceeds the fine-structure splitting the adiabatic potentials $V(R)$ that separate to the $3P_{J,M_J}$ state do not depend on M_S or M_l of the perturber, i.e., the D_2 diatomic states that separate to Na* simplify into three $V(R)$ that only depend on J, M_l, and M_S of the Na*. However, the Na fine-structure operator as well as the van der Waals energies must be included in evaluating these $V(R)$. We therefore calculate C_6 coefficients for sodium n,L,M_L states, which we label $C_6(n,L,M_L)$, then diagonalize the combined fine-structure and $-C_6(n,L,M_L)R^{-6}$ operators to obtain the adiabatic long-range potentials. In the region where ΔE (fine-structure) $\gg C_6R^{-6}$, these long-range potentials follow $-C_6(n,L,J,M_J)R^{-6}$; at smaller R they recouple to follow $-C_6(n,L,M_J)R^{-6}$.

Gallagher and Holstein[18] Eqs. (A3) and (A4), with $M_1=L_1=0$, yields $C_6(\alpha)$ in atomic units for an alkali-metal-atom (A) state $\alpha=n,L,J,M$ against an S-state perturber (atom B, with ground state gS and excited $n''P$ states)

$$C_6(n,L,J,M)=\sum_{n''}\left[\frac{2[R(B)]^2_{g,n''}}{3}\right]\sum_{\mu,n',L',J',M'}\frac{2}{[1+3\mu^2]}\begin{pmatrix}J' & 1 & J\\ -M' & \mu & M\end{pmatrix}^2\frac{(2J+1)(2L+1)(2J'+1)(2L'+1)}{\Delta E(a)+\Delta E(B)}$$
$$\times\begin{Bmatrix}L' & J' & S\\ J & L & 1\end{Bmatrix}^2\begin{Bmatrix}L' & 1 & L\\ 0 & 0 & 0\end{Bmatrix}^2[R(A)]^2_{nL,n'L'}\,, \tag{B1}$$

where $\Delta E(2)=E_n(2)-E_g(2)$, $\Delta E(1)=E_{n'L'}-E_{nL}$, and $[R(i)]_{\alpha,\beta}$ is the radial integral of electron coordinate r for atom i.

To obtain the $C_6(n,J,M_L)$ we take $S=0$ in Eq. (B1):

$$C_6(n,L,M_L)=\sum_{n'',n',L',\mu}\left[\frac{2[R(2)]^2_{g,n''}}{3}\right]\frac{2[R(1)]^2_{nL,n'L'}}{1+3\mu^2}\begin{pmatrix}L' & 1 & L\\ -M' & \mu & M\end{pmatrix}^2(2L+1)(2L'+1)\begin{pmatrix}L' & 1 & L\\ 0 & 0 & 0\end{pmatrix}^2. \tag{B2}$$

For $L=1$, $L'=0$ and two terms in (B2) can be grouped to obtain

$$C_6(n,L=1,M_L)=D\frac{22-3M_L^2}{20}+S\frac{2}{1+3M_L^2}\,, \tag{B3}$$

where

$$D=\sum_{n'',n'}\left[\frac{2[R(2)]^2_{g,n''}}{3}\right]\frac{(2/3)[R(1)]^2_{nl,n'2}}{\Delta E(1)+\Delta E(2)}$$

results from the sum over $L'=2$ state (D states), and

$$S=\sum_{n'',n'}\left[\frac{2[R(2)]^2_{g,n''}}{3}\right]\frac{(1/3)[R(1)]^2_{n1,n'0}}{\Delta E(1)+\Delta E(2)}$$

is from the sum over $L'=0$ states (S states).

D and S can be reexpressed in terms of absorption oscillator strengths using

$$f_{1-2}=\frac{2}{3}\frac{l_>}{2l_l+1}(\Delta E)R^2_{1,2}\,,$$

where ΔE and R^2 are in atomic units, l_l is the orbital angular momentum of the lower state, and $l_>$ of the state of largest angular momentum. We now specialize to C_6 for the first excited state, so that all D states have higher energies, to obtain

$$D=\tfrac{3}{2}\sum_{n'',n'}\frac{[f(2)]_{gS-n''P}}{[\Delta E(2)]_{gS-n''P}}\frac{[f(1)]_{nP-n'D}}{[\Delta E(1)]_{nP-n'D}}\times\frac{1}{\Delta E(2)+\Delta E(1)}\,. \tag{B4}$$

Since only the ground state (nS) has lower energy than the nD state, we take $S=S_0+S_1$, where S_0 comes from this $n'=n$ term and S_1 from all other (higher S-state) terms:

$$S_0=\tfrac{1}{2}\sum_{n''}\frac{[f(2)]_{gs-n''P}}{[\Delta E(2)]_{gs-n''P}}\frac{[f(1)]_{np-ns}}{[\Delta E(1)]_{np-ns}}\times\frac{1}{\Delta E(2)+\Delta E(1)}\,,$$

$$S_1=\tfrac{3}{2}\sum_{n'',n'>n}\frac{[f(2)]_{gs-n''p}}{[\Delta E(2)]_{gs-n''p}}\frac{[f(1)]_{np-n's}}{[\Delta E(1)]_{n'p-ns}}\times\frac{1}{\Delta E(2)+\Delta E(1)}\,.$$

The first term in S_0 is the nearly resonant interaction between, for example Na*Rb and NaRb*, and the denominator $\Delta E(2)+\Delta E(1)$ is very small for this term. The denominator is positive for the lower state (e.g., NaRb*), and negative for the higher state (e.g., Na*Rb), so that $\Delta E=-C_6R^{-6}$ repels these states. [For alkali-metal perturbers only the first ($n''=g$) term is significant in D, S_0, and S_1.] Values of D, S_0, and S_1, evaluated from known alkali-metal oscillator strengths, are given in Table III for the Na $3P$ state against various alkali-metal perturbers.

When Eq. (B1) is evaluated for $S=\frac{1}{2}$, $L=1$, we obtain

$$C_6(J=\tfrac{3}{2},M_J)=\frac{21.25-M_J^2}{20}D+(2-|M_J|)(S_0+S_1)\,, \tag{B5a}$$

$$C_6(J=\tfrac{1}{2},M_J=\tfrac{1}{2})=D+S_0+S_1\,. \tag{B5b}$$

These and the $C_6(M_L)$ are tabulated in Table III. Note that the M_L average of Eq. (B3), the M_J average of (B5a)

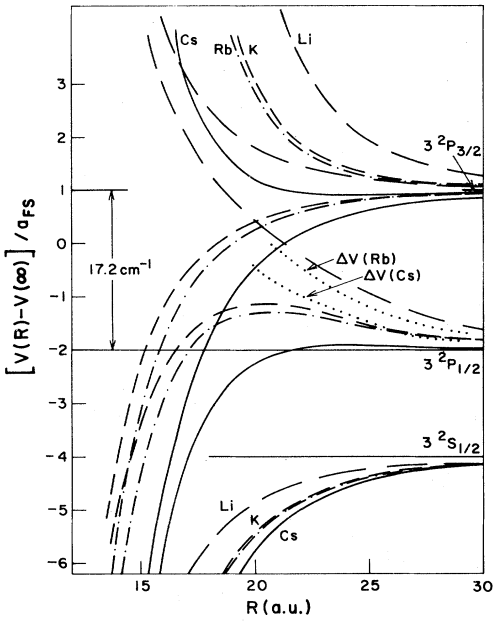

FIG. 7. Na $3S$-$3P$ state interactions with dissimilar alkali-metal atoms due to the fine-structure interaction plus dipole-dipole dispersion forces (Appendix B).

and (B5b) all equal $D+S$. Also, Eq. (B3) with $M_L=1$ is the same as Eq. (B5a) with $M_J=\frac{3}{2}$, as expected since the latter is a pure $M_L=1$ state.

When the fine-structure operator, $2a\vec{L}\cdot\vec{S}/3$, plus the $-C_6(3P,M_L)R^{-6}$ operators (diagonal in M_L and M_S) are simultaneously diagonalized, the energies of the states that separate to $3^2P_J,M_J$ are given by E_{J,M_J}:

$$
\begin{aligned}
E_{3/2,3/2}&=\tfrac{1}{3}a(1+\beta y)\ ,\\
E_{3/2,1/2}&=\tfrac{1}{6}a\{-1+(1+\beta)y+[(1+(\beta-1)y^2+8]^{1/2}\},\\
E_{1/2,1/2}&=\tfrac{1}{6}a\{-1+(1+\beta)y\\
&\qquad -[(1+(\beta-1)y)^2+8]^{1/2}\}\ .
\end{aligned}
\tag{B6}
$$

Here $y=-3C_6(3P,M_L=0)/aR^6$, $\beta=C_6(3P,M_L=1)/C_6(3P,M_L=0)$, and a is the Na(3^2P) fine-structure interval (17.2 cm^{-1} or 7.8×10^{-5} a.u.). For small y (large R), Eq. (B6) reduces to $E_{J,M_J}=E_{3P_J}-C_6(3P_J,M_J)R^{-6}$, and for large y (small R) the states approach M_L eigenfunctions with energies $E_{3P}-C_6(3P,M_L)R^{-6}$. These adiabatic energies and that of the ground state are shown through the recoupling region in Fig. 7. The $\Delta V=V(3P_{1/2,M_J})-V(3^2S_{1/2})$ for Na-Rb and Na-Cs are plotted in Fig. 7 as dots in the long-range region relevant to the line broadening reported here.

*Present address: Fachbereich Physik der Freien Universität, Arnimallee 14, D-1000 Berlin 33, West Germany.
†Present address: Institut für Experimentalphysik der Universität Kiel, D-2300 Kiel, West Germany.
‡Quantum Physics Division, National Bureau of Standards.

[1]E. L. Lewis, Phys. Rep. 58, 1 (1980).
[2]C. G. Carrington, D. N. Stacey, and J. Cooper, J. Phys. B 6, 417 (1973).
[3]M. Movre and G. Pichler, J. Phys. B 13, 697 (1980).
[4]E. E. Nikitin, in *The Excited State in Chemical Physics,* edited by J. W. McGowan (Wiley, New York, 1975), Chap. V.
[5]L. Krause, in *The Excited State in Chemical Physics,* (Ref. 4), Chap. IV.
[6]R. Beuc, M. Movre, and C. Vadla, J. Phys. B 15, 1333 (1982).
[7]P. J. Bertoncini, G. Das, and A. C. Wahl, J. Chem. Phys. 52, 5112 (1970).
[8]R. E. Olson, private communication.
[9]H. Chatham, E. L. Lewis, and A. Gallagher, J. Phys. B 13, L7 (1980); note that Γ is in frequency units, actually corresponding to $\Gamma/2\pi$.
[10]J. Szudy and W. E. Baylis, J. Quant. Spectrosc. Radiat. Transfer 15, 641 (1975).
[11]R. Walkup, A. Spielfiedel, D. Ely, W. Phillips, and D. Pritchard, J. Phys. B 14, 1953 (1981).
[12]C. L. Chen and A. V. Phelps, Phys. Rev. 173, 62 (1968).
[13]J. Huennekens and A. Gallagher, Phys. Rev. A 27, 1851 (1983).
[14]A. N. Nesmeyanov, *Vapor Pressures of the Chemical Elements* (Elsevier, New York, 1963).
[15]E. L. Lewis and A. Gallagher, J. Opt. Soc. Am. 63, 864 (1973).
[16]C. Vadla, Ph.D. thesis, University of Zagreb, Yugoslavia 1982 (unpublished).
[17]A. Mitchell and M. Zemansky, *Resonance Radiation and Excited Atoms* (Cambridge University Press, London, 1934). The appendix treats a single Doppler line; the Na hfs causes a minor increase in $k_{\rm eff}/k_0$.
[18]A. Gallagher and T. Holstein, Phys. Rev. A 16, 2413 (1977).